Observing planets and small bodies in sputtered high-energy atom fluxes

A. Milillo,[1] S. Orsini,[1] K. C. Hsieh,[2] R. Baragiola,[3] M. Fama,[3] R. Johnson,[3] A. Mura,[1] C. Plainaki,[1] M. Sarantos,[4] T. A. Cassidy,[5] E. De Angelis,[1] M. Desai,[6] R. Goldstein,[6] W.-H. Ip,[7] R. Killen,[8] and S. Livi[6]

Received 4 February 2011; revised 15 April 2011; accepted 25 April 2011; published 30 July 2011.

[1] The evolution of the surfaces of bodies unprotected by either strong magnetic fields or thick atmospheres in the solar system is caused by various processes, induced by photons, energetic ions, and micrometeoroids. Among these processes, the continuous bombardment of the solar wind or energetic magnetospheric ions onto the bodies may significantly affect their surfaces, with implications for their evolution. Ion precipitation produces neutral atom releases into the exosphere through ion sputtering, with velocity distribution extending well above the particle escape limits. We refer to this component of the surface ejecta as sputtered high-energy atoms (SHEA). The use of ion sputtering emission for studying the interaction of exposed bodies (EB) with ion environments is described here. Remote sensing in SHEA in the vicinity of EB can provide mapping of the bodies exposed to ion sputtering action with temporal and mass resolution. This paper speculates on the possibility of performing remote sensing of exposed bodies using SHEA and suggests the need for quantitative results from laboratory simulations and molecular physic modeling in order to understand SHEA data from planetary missions. In Appendix A, referenced computer simulations using existing sputtering data are reviewed.

Citation: Milillo, A., et al. (2011), Observing planets and small bodies in sputtered high-energy atom fluxes, *J. Geophys. Res.*, *116*, A07229, doi:10.1029/2011JA016530.

1. Introduction

[2] Studying the evolution of the surfaces and atmospheres of bodies in the solar system is fundamental to our understanding of the present composition of planetary surfaces and atmospheres. This endeavor entails finding how the rates of the ongoing processes vary as a function of the space environment. Aside from occasional catastrophic events, such as volcanic eruptions in a few bodies or occasional collisions with comets and asteroids, surface and atmospheric changes are caused predominantly by the continuous bombardment of the bodies by photons, energetic ions and micrometeoroids. Yet the actual effects of these incident fluxes on the present state of planetary bodies are not well described. To investigate this complex topic, we propose to begin with a much simpler quest by focusing on the subset of planets, moons and small bodies that are not protected by either strong magnetic fields or thick atmospheres. For surfaces of exposed bodies (EB) such as Mercury, Moon, and asteroids, directly exposed to the solar wind, the alteration of the solid surface and the production of the surface-bound exospheres by the impacts of the time-varying solar wind (SW) over the last 4.54 Gy constitute a relevant component of space weathering. For other EB, such as Callisto, Europa and Ganymede of Jupiter, energetic magnetospheric (MS) ions play the major role in altering the respective surfaces and atmospheres. Hence, we shall focus on the process of ion sputtering (IS) on EB, i.e., on bombardment by either SW or MS ions.

[3] In the past, the nature of space weathering has been reviewed in detail and the sputter alteration of regoliths of outer solar system bodies has been discussed [*Hapke*, 1986, 2001]. Moreover, a mathematical theory describing the optical effects of space weathering has been derived and applied to the regoliths of the Moon, Mercury and an S asteroid [*Hapke*, 2001]. Whereas *Hapke* [2001] discussed the spectral effects and the melting of minerals caused by space weathering, in this study we consider as its main specific signature the flux of energetic atoms ejected upon impact of energetic particles on the surfaces.

[4] Although there are other surface-ejected atoms and molecules, such as those released by thermal desorption (TD), photon-stimulated desorption (PSD) and micrometeoroid impact vaporization (MIV), we shall show that IS ejecta produced by the incident SW or MS ions provide a unique

[1]INAF/IFSI, Rome, Italy.
[2]Department of Physics, University of Arizona, Tucson, Arizona, USA.
[3]Materials Science and Engineering, University of Virginia, Charlottesville, Virginia, USA.
[4]Heliophysics Division, NASA GSFC, Greenbelt, Maryland, USA.
[5]Jet Propulsion Laboratory, Pasadena, California, USA.
[6]Southwest Research Institute, San Antonio, Texas, USA.
[7]Department of Astronomy, National Central University, Jhongli, Taiwan.
[8]Planetary Magnetospheres Division, NASA GSFC, Greenbelt, Maryland, USA.

Copyright 2011 by the American Geophysical Union.
0148-0227/11/2011JA016530

window to observe space weathering of EB. These ions may be partly neutralized and backscattered from the surface to space (up to 20% for light ions like the SW major components [see *McComas et al.*, 2009; *Wieser et al.*, 2009]), but a significant fraction of the incident ions, increasing with ions atomic mass number, can be implanted on the EB surface while ejecting a surface atom or molecule. Sputtering products from impacts of keV ions can have energies, peaking at few eV with a high-energy non-Maxwellian tail, up to at least several tens eV for a refractory material [*Goehlich et al.*, 2000]. We refer to this component of the surface ejecta as sputtered high-energy atoms (SHEA). At these energies, SHEA emitted from regolith can easily escape the local gravity (e.g., 0.09 eV/nucleon for Mercury and 0.03 eV/nucleon for the Moon) and be distinguished from other surface-released products from TD, PSD and MIV, all typically ≤1 eV. *Plainaki et al.* [2010] show that even in the case of icy moons the flux of escaping IS ejecta is significantly higher than the other products (see also Figure A4). The energy spectra of SHEA, of course, strongly depend on the incident flux and surface composition. Being electrically neutral and energetic, SHEA can escape both the magnetic and gravitational field present between their places of birth (where sputtering occurs) and a SHEA analyzer onboard either an orbiter or a flyby probe. If, on the same spacecraft, the SW or MS ions are monitored by a plasma analyzer and the surface composition of the exposed bodies (EB) analyzed by IR, X-ray, γ ray or neutron spectrometers, then the detection of mass and energy distributions of SHEA would provide the missing piece in determining the magnitude and rate of space weathering of the given EB's surface as well as the composition of its surface-bound exosphere.

[5] Recent observations of heavy pickup ions at Mercury by the MESSENGER spacecraft [*Zurbuchen et al.*, 2008] and the pickup ions from reflected SW protons at the Moon by the Kaguya spacecraft [*Saito et al.*, 2008] have shown most clearly that SW-ion and EB-surface interactions are a link between the physics of space plasma and of surface-bound exospheres. Furthermore, Chandrayaan-1 Energetic Neutrals Analyzer (CENA) was, in principle, able to measure neutral atoms of 10 eV to 3 keV [*Bhardwaj et al.*, 2005]. This sensor observed an energetic neutral signal from the Moon surface, interpreted as the product of neutralization and backscattering of the solar wind, probably prevailing on sputtering signal at the Moon [*Wieser et al.*, 2009]. The results and sensitivity of CENA could provide an indication for estimating an upper limit of the flux of SHEA around the Moon. These recent results come, however, from in situ measurements of the already processed surface releases. Were remote sensing of the surface via SHEA from the vicinity of Mercury and of Moon with appropriate instrumentation available, then more direct and detailed investigations could be done on the nature of the surface-plasma interaction under different physical conditions, e.g., SW condition, solar radiation effect, magnetospheric condition, and surface property. Such investigations may be carried on by monitoring SHEA flux intensity, emitting area extension and particle relative abundances. The comparison between the ground-based observations and spacecraft measurements and between pickup ion and SHEA measurements would resolve many outstanding issues such as the interplay between ion sputtering and photodesorption by solar UV photons, the relative importance of thermal desorption and meteoroid impact as source mechanisms of the sputtered exospheric atoms.

[6] Clearly, to accurately interpret any SHEA data from space weathering effects on surfaces of EB will require active participation of physicists doing sputtering experiments in laboratories directly applicable to the interactions between SW or MS ions and EB surfaces. Only such experiments can quantify the microscopic processes controlling the sputtering yield Y_i, the number of released particles per incident ion, basic to remote sensing in SHEA.

[7] Remote sensing EB via SHEA by orbiters or flyby probes can also provide information to complement the observations from Earth or by instruments landed on these solid bodies. Although flyby missions offer only brief observation of one body, each mission could be planned to flyby several bodies. The advantage of orbiters over landers, besides cost, is its global survey under varying conditions over longer time periods. In the case of orbiting larger planets with many moons, the ability to observe several moons has been successfully demonstrated by missions Galileo and Cassini. These and other orbiter missions, unfortunately, are not equipped to study space weathering of the EB. To examine the issue of SHEA capability on future EB missions, an in-depth discussion is necessary.

[8] To begin this discussion, we start with the data and techniques currently available to assess whether or not SHEA instruments are critical to future orbiter or flyby missions. To this end, details are presented in the following manner: the production of SHEA in section 2, justification for SHEA observation in section 3, the need for laboratory-based ground truth in sputtering in section 4, and the conclusions in section 5. Examples of computer simulations of SHEA emissions from Mercury, Moon, asteroids and Jovian Moons, based on existing data and theories, are presented in Appendix A.

2. Production of SHEA

[9] The IS results from the impact of an ion of mass m_1 onto a solid surface. If the ion incident energy E_i is high enough, surface atoms may be ejected. Some IS processes producing SHEA are represented in Figure 1. For oblique incidence, ion sputtering can be a single-step process, often called "knock-on," in which the ions directly eject surface atoms (Figure 1a). Otherwise, a multistep process takes place, often called "collision cascade" (Figure 1d). Light incident ions are often backscattered in layers near the surface, and occasionally they may be neutralized in the process before returning to space (not shown), but would be like in Figure 1e without the second collision. Backscattered ions can trigger a cascade of collisions among atoms close to the surface. While the heavy incident ions produce forward-directed recoils.

[10] The energy transferred in the first collision to a surface atom is given by classical mechanics:

$$T = T_m \cos^2 \alpha_r$$
$$T_m = E_i \frac{4\, m_1 m_2}{(m_1 + m_2)^2}, \quad (1)$$

where E_i and m_1 are the incident ion energy and mass, respectively, m_2 is the mass of the struck atom (the recoil),

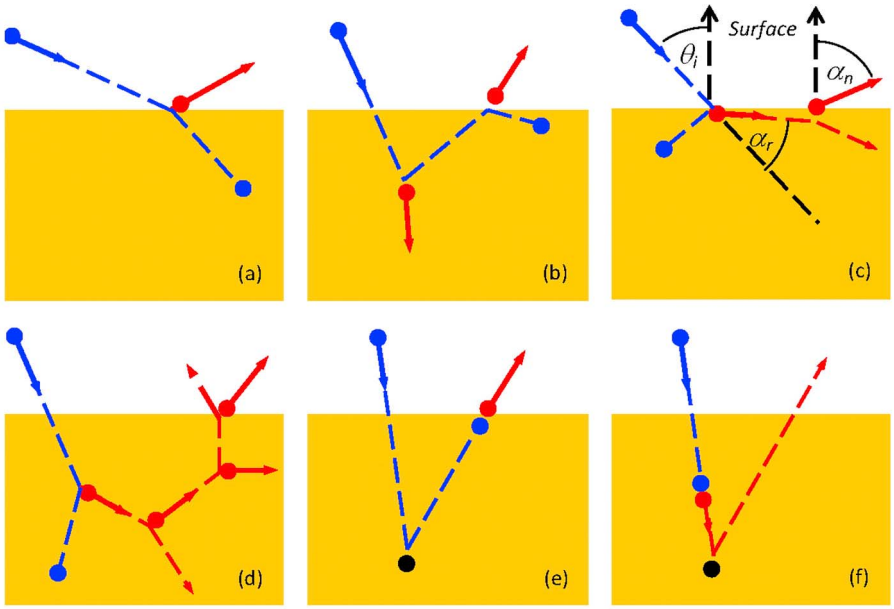

Figure 1. Examples of ion-induced SHEA ejection. Incident energetic ions are blue, and atoms of the exposed surface are red. Ejections shown are by (a) primary or first recoil, (b) knock-on by a backscattered ion without a cascade, (c) secondary recoil, (d) higher-order recoil or cascade, (e) backscattered incident ion, and (f) backscattered recoil atom. Figures 1e and 1f are for surfaces having more than one element, e.g., more massive atoms (black). The angles shown in Figure 1c define the directions of the incident ion, the recoil atom, and the ejected SHEA. Figures 1b and 1e are indistinguishable externally, except in the energy of the SHEA. Based on Figure 2.1 of *Sigmund* [1981] and Figure 2.6 of *Hofer* [1991].

T the energy transfer, T_m its maximum value, and α_r the scattering angle of the recoil atom (see Figure 1). Collisions below the surface layer involve both the projectile and the recoil atoms, with the cascade of collisions eventually leading to sputtering, i.e., the ejection of an atom or molecule from the solid. For a regolith material (independently of composition or porosity), the ejected particles are mostly neutral atoms [*Hofer*, 1991]. For ejected atoms or molecules of species n with partial sputtering yield Y_n, the normalized distribution of ejecta ($f_{S,n}$) from a refractory material, as a function of ejecta energy E_e, can peak at few eV [*Gnaser*, 2007; *Hofer*, 1991] and can often be empirically reproduced by the following function [*Sigmund*, 1969; *Sieveka and Johnson*, 1984]:

$$f_{S,n}(E_e, E_i, \alpha_n) = c_n \frac{E_e}{(E_e + E_{b,n})^3}\left[1 - \sqrt{\frac{E_e + E_{b,n}}{T_m}}\right]\cos\alpha_n, \quad (2)$$

where $E_{b,n}$ is the surface binding energy of the ejected atoms, α_n the polar angle of the SHEA with respect to the surface normal (Figure 1), and c_n the normalization constant. *Gnaser* [2007] showed that the effective binding energy $E_{b,n}$ is typically lower than the bulk cohesive energy. For refractory materials, the difference between the two can be as much as 50%, but more typically ~10–20%. For volatile materials that dominate the outer solar system, the difference can be an order of magnitude [e.g., *Reimann et al.*, 1984; *Johnson et al.*, 2011]. Empirically, all variables in equation (2) can be measured, except $E_{b,n}$. By fitting equation (2) to laboratory data on sputtering, therefore, can uniquely determine $E_{b,n}$.

[11] Samples for comparing computed with measured $f_{S,n}$ as functions of E_e for different incident ions and solid targets are shown in Figure 2. Figures 2a and 2b are $f_{S,n}$ computed for Na ejected by protons incident on a planetary-like mineral for different values of $E_{b,Na}$ and of E_i, respectively, using equation (2) averaged over angle α_n [*Sigmund*, 1969; *Sieveka and Johnson*, 1984]. It is clear that E_i sets the upper limit on E_e, while E_b affects the energy at which the distribution peaks. Figure 2c shows good agreement between Monte Carlo SRIM [*Ziegler et al.*, 1966] simulation results (for a surface composition derived by *Goettel* [1988]) and equation (2) in the high-energy tail in the case of 1 keV protons on a planetary-like surface. Moreover, Figure 2d compares equation (2) with experimental results of Ar^+ impacting on W at four different values of E_i for $\theta_i = \alpha_n = 0$ [*Goehlich et al.*, 2000, Figure 3] with equation (2); the agreement improves for $E_i > 500$ eV. The spectrum of the ejected Na shown in Figure 2e is converted from velocity to energy E_e as the independent variable, resulting from bombarding a Na_2SO_4 target with 3.5 keV Ar^+, as might be the case for surfaces of Io [*Wiens et al.*, 1997] or, possibly, certain regions of Europa although Na is often in an ice matrix [e.g., *Johnson*, 2002]. The spectrum fits the form of equation (2), which has a measured tail extending to a few eV, but peaks at ~0.3 eV, well below that shown in Figure 2d. They also showed that the Monte Carlo SRIM is able as well to reproduce the process for different impact energies and angles. Figure 2f gives the energy spectra of sputtered D_2O and SO_2 from 5 keV Ar^+ impacting a heavy water ice matrix containing SO_2 [*Johnson et al.*, 2011]. Figure 2 demonstrates the wide applicability of equation (2), except for the lowest-energy portion shown in Figure 2f, as explained by *Johnson et al.* [2011], and the need to establish $E_{b,n}$ for incident ions

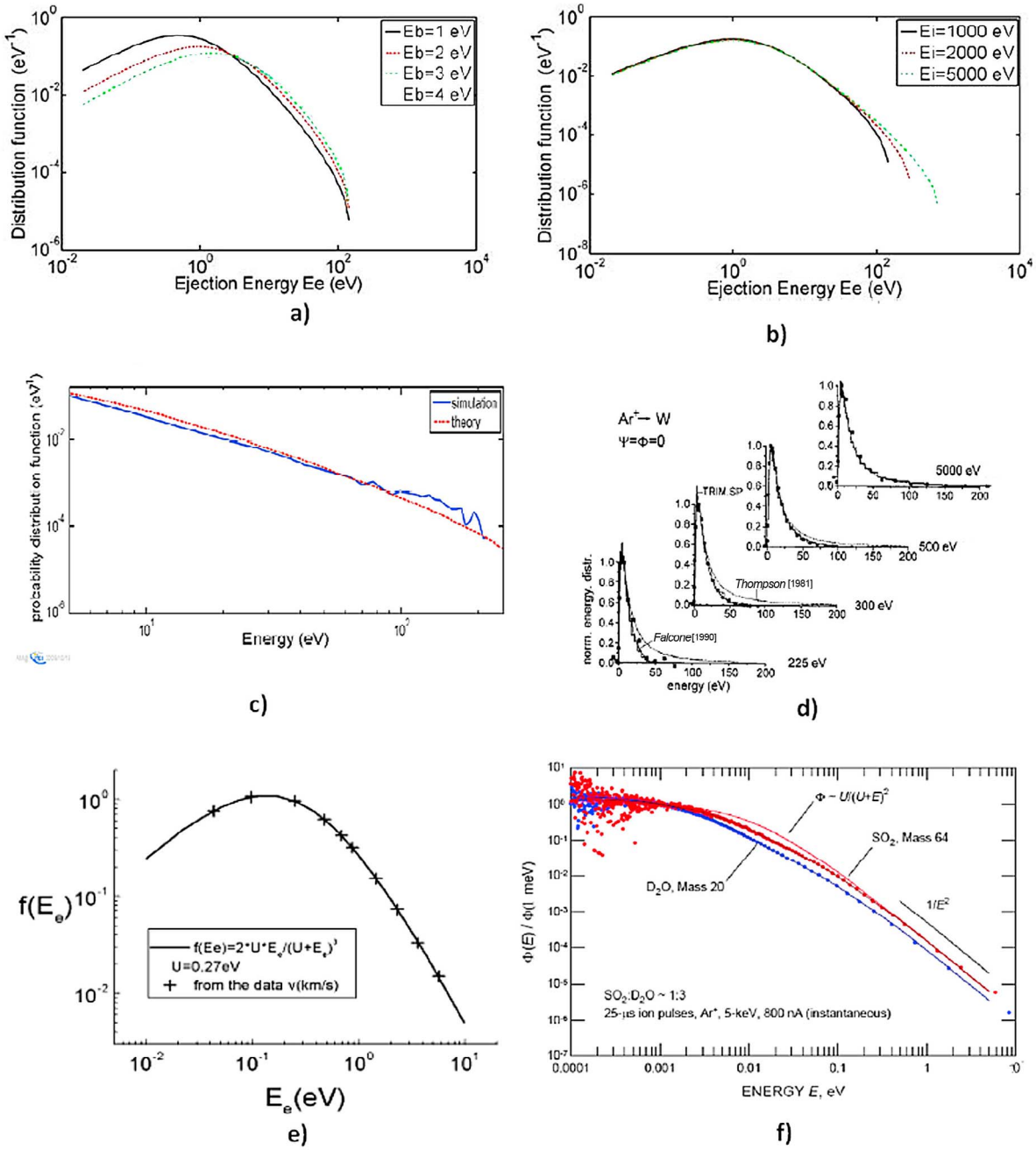

Figure 2. Some measured and computed SHEA spectra. (a) Computed energy distribution function $f_{S,n}$ (equation (2)) of Na sputtered from 1 keV protons impacting on a simulated planetary-like mineral surface for different assumed Na binding energies. (b) Computed $f_{S,n}$ of Na ejecta, assuming a 2 eV binding energy, for protons of different energies impacting on regolith-like simulated (again regolith means the porosity was accounted for). (c) Comparison of high-energy part of Na ejecta distribution (dashed line) and SRIM simulations (solid line, for the assumed surface composition [see *Goettel*, 1988]) for E_i = 1 keV. (d) SHEA energy spectra for Ar^+ of different E_i on W at zero incident and ejection angles [*Goehlich et al.*, 2000]. (e) Ejection of Na from Na_2SO_4 for impacting Ar^+ of 3.5 keV and with E_b ~ 0.27 eV [*Wiens et al.*, 1997]. (f) Sputtering of D_2O ice with ~30% SO_2 bombarded by 5 keV Ar^+. Energy profile of sputtered SO_2 (red dots) and D_2O (blue dots) molecules, normalized at 1 meV flux. The energy profiles are fit to two distributions of the form $E_b/(E_e + E_b)^2$. The fit shows for DO_2 (blue, lower curve) U ~ 0.048 eV for a fraction 0.32 of the molecules ejected with U ~ 0.0033 eV for the remainder; for the SO_2 component (red, curve over the dots), U ~ 0.043 eV for a fraction 0.36 of the ejected molecules, with U ~ 0.0053 for the remainder [*Johnson et al.*, 2011].

and targets relevant to the study of space weathering of selected EB.

[12] The angular distribution of the ejected atoms depends on the incident ion mass so that a general expression is not easily defined; detailed discussions can be found in work by *Hofer* [1991] and *Gnaser* [2007]. For heavy incident ions, the ion impact direction does not have a large effect on the distribution in ejection angle α_n, which is often approximated $\cos^k(\alpha_n)$, where k is usually between 1, as in equation (2), and 2. For light ions, the angular distribution is related to the ion impact direction, and exhibits a maximum close to the mirroring angle. For a surface composed of a number of different atomic species, the angle-averaged differential flux of sputtered atoms is

$$\frac{d\Phi}{dE_e} = \sum_n C_n \int_{E_{\min}}^{E_{\max}} \frac{d\Phi_I}{dE_i} Y_n f_{s,n}(E_e, E_i) dE_i, \quad (3)$$

where C_n is the relative surface abundance of the atomic species n, and Φ_I is the incident ion flux. The total sputtering yield $Y = \int (d\Phi/dE_e) dE_e$, in general, depends on the impinging ion mass and energy and on the surface mineralogy. Averaged over the solar wind ion energies, Y can range from 0.01 to 0.1 [*Lammer et al.*, 2003; *Johnson and Baragiola*, 1991] for refractory surfaces, whereas it ranges in between 10 and 1000 for icy surfaces of the Jovian moons when bombarded by hundreds keV MS heavy ions [*Johnson*, 1990; *Famá et al.*, 2008; *Johnson et al.*, 2011]. These values are reduced by the regolith porosity [*Cassidy and Johnson*, 2005]. The yield is also a function of the incident ion's mass and nuclear charge. In general, every precipitating ion contributes to sputtering from the EB surface. For example, accounting for the solar wind abundance of the ions, the net sputtering rate generated by protons with respect to other solar wind components, like α particles or high charge state particles, is estimated to be comparable [*Johnson and Baragiola*, 1991]. In the case of the icy moons of the giant planets hit by heavy and energetic magnetospheric plasma ions, the ejecta are dominated by low-energy atoms and molecules. Since the yields from such surfaces can be large, both simulations [*Cassidy et al.*, 2009] and experiments [*Johnson et al.*, 2011] show that the trace species are carried off with the ice matrix. The two sets of EB, one exposed to SW only and the other exposed predominantly to magnetospheric plasma, make a comparative study that would improve our understanding of the mechanism of space weathering.

3. The Uniqueness of SHEA Observation

3.1. Selecting a Starting Point in the Study of Surface Evolution

[13] The understanding of the role played by SW and MS ions, solar radiation and micrometeorites in bombarding, in altering the surfaces and atmospheres of these bodies, as well as the determination of the mass loss rate of the respective bodies [*Killen and Ip*, 1999; *Madey et al.*, 2002] provides a relevant contribution to the study of the evolution of solid bodies of the Solar System. To begin this ambitious and challenging study, we have, as stated in section 1, selected the EB in the solar system that are not protected by either strong magnetic fields or thick atmospheres. Such bodies are directly exposed to the incident radiations, and the resulting released atoms and molecules can escape with least hindrance. On the other hand, those atoms that fail to escape populate the surface-bound exospheres [e.g., *Johnson*, 2002]. The choice of EB also minimizes interference, such as deflection by strong local magnetic fields or/and scattering by intervening atmospheric particles, on the incident radiation as well as on the ejecta from the site of impact.

[14] Among the processes occurring on the surfaces of EB, which include TD, PSD, IS and MIV, we select, also stated in section 1, IS (ion sputtering) the first process for investigation. Our choice of IS on EB to begin our study on surface evolution is not just because we recognize the principal role of the time-varying ion flux intensity over the last 4.54 Gy in space weathering of bodies in our solar system [*Orsini et al.*, 2009a], but also due to the fact that three necessary sets of observables can be made accessible. These complementary observables are: the incident radiation, which has been and will continue to be monitored by planetary missions; the surface composition and mineralogy of EB, which have been and should be investigated by spaceborne X-ray, IR, neutrons, and gamma ray spectrometers; and the ejecta of IS, which have distinct features that favor direct and precise detection and analysis, but yet to be implemented. Recently, Kaguya and Chandrayaan-1 spacecraft had X-Ray, IR, neutrons, gamma ray and particle analyzers. Although Kaguya particle analyzers measure only ions and electrons, some of SHEA are ionized. A joint analysis of these kinds of observations could provide hints in this study. The future BepiColombo Mission, already including in its payload all these sensors and especially a dedicated SHEA detector, promises outstanding outcomes (see section A1).

3.2. SHEA Detection for Observing Space Weathering

3.2.1. Energetically Distinct

[15] Different release processes produce particles within different energy ranges [*Wurz and Lammer*, 2003; *Milillo et al.*, 2005; *Leblanc and Johnson*, 2010]. The ejected atoms and molecules, depending on their velocity, can either return to the surface, become part of the atmosphere, escape the gravitational field, or be photoionized and picked up by planetary magnetospheres. The velocity distributions are different for the relevant processes, and thus can serve as important signatures of the processes involved. TD and PSD are more effective for volatiles (like H, He, Na, K, S, Ar) and have typical energy below 1 eV (dashed lines in Figure 3, left and middle refer to 2 eV Na, that is, the escape energy at Mercury), while IS and MIV are effective also for refractory species (e.g., Mg, Al, Si, and Ca), thus producing more energetic ejecta closer to stoichiometric composition. In contrast to the MIV-released particles having a Maxwellian distribution of an expected peak corresponds to ~2500–5000 K [*Eichhorn*, 1978] or a peak particle energy of ~0.6 eV, the high-energy tail of IS ejecta, SHEA, on the other hand, can in principal have surface release energies above 10 eV [*Gnaser*, 2007; *Wiens et al.*, 1997], more than sufficient to escape the local gravity (e.g., 0.09 eV/nucleon for Mercury, 0.03 eV/nucleon for Moon). This means that releases from all other processes can be excluded, when analyzing IS products through SHEA detection (Figures 3, right and 2). Nevertheless, the escape fraction of released particles depends on each specific case (escape velocities, main release processes, surface properties, external conditions) and it is a complicated

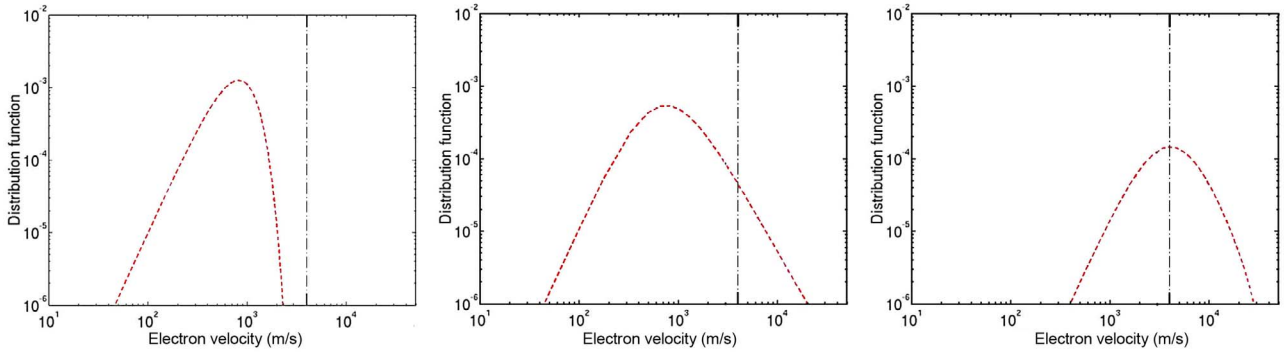

Figure 3. Model of velocity distribution functions for (left) TD, (middle) PSD, and (right) IS (adapted from *Killen et al.* [2007]). See also Figure 2 for SHEA spectra. Dashed lines correspond to the Na escape energy at Mercury equal to 2 eV, for reference.

quantity to estimate. Generally, one of the main processes responsible for the total surface material loss rate is IS, but minor contribution can be due to radiation pressure for specific species and to the other release processes, as well.

[16] SHEA may also be distinguished from backscattered atoms (BSA). This population is not a negligible fraction of material leaving the surface, but definitely not of surface composition. BSA are just neutralized impacting ions that are reflected back from the surface, so that their energy is comparable to that of the incident ions. Backscattering is much more efficient for light species, like H, so that both their flow velocity and energy are well separated from those characterizing the IS ejecta, SHEA. This means that an instrument is able to discriminate between these two signals provided that its ToF or energy resolution is high enough. If we consider 1 keV proton onto regolith surface, we can assume a total yield of ion sputtering about 10%, and that of backscattering about 20%, then, the expected fluxes are comparable.

[17] SHEA mapping on EB is distinctly different from ENA (energetic neutral atoms) imaging remote plasma such as planetary magnetospheres or moons [e.g., *Hsieh and Curtis*, 1988; *Krimigis et al.*, 2004]. The latter relies on the production of energetic atoms by charge exchange between energetic ions and ambient atoms and molecules along the line of sight and within the solid angle of the ENA imager. The intensity of charge exchange ENA flux is, therefore, a column density measurement along the line of sight. The choice of EB as the solid target and IS as the process effectively renders any ENA produced along the line of sight between EB and the SHEA detector insignificant, because the charge exchange cross section typically $<10^{-14}$ cm^2 for ~10 eV ions [e.g., *Lindsay and Stebbings*, 2005], the number density of atoms in interplanetary space is $\sim 10^{-1}$ cm^{-3} [e.g., *Bzowski et al.*, 1996, 2008], and distance between EB surface and the observing spacecraft (s/c), hence the path length for ENA, $\sim 10^{2-3}$ km. Hence, the product of these three quantities indicates that the maximum ENA flux that can reach the observing s/c from the observed EB would be $\sim 10^{-6}$ of the ambient ion flux. This is orders of magnitude smaller than the expected SHEA flux under the bombardment of the same ion flux, due to the fact that the all species–integrated sputtering yield is of the order 0.1, in the case of a regolith surface hit by 1 keV proton. Moreover, ion fluxes at 10 eV are usually negligible in the EB environment; generally, charge exchange ENA are in the keV range, when the plasma is mainly SW, or they can have higher energies when considering the giant planets magnetospheres, and ion directions are generally not from the body to the s/c. So the expected ENA flux comes from different directions and at different energy range from those of SHEA.

[18] Having distinguished SHEA from backscattered neutrals, charge exchange ENA and ejecta of other surface-altering processes, we arrive at the unique advantage of observing targeted EB in SHEA.

3.2.2. SHEA Mapping: Instantaneous and Localized

[19] While the ground-hugging exospheres of EB maybe a mixture of lingering releases from all other surface processes over time, escaping SHEA, on the other hand, travel ballistic trajectories from their ejection sites or ion impact site to the observing spacecraft, thus carrying instantaneous and localized information on their origins. SHEA enable us to directly map the spatial distribution of the ion impact flux in time. Correlating observed time profile of SHEA with that of the impinging ions, e.g., SW or MS ions, bombarding the surface, with the knowledge of surface composition provided by means mentioned in the beginning of section 2, it is not difficult to imagine how the specific yield and erosion rate could be obtained, within the time-spatial and mass resolution of the SHEA instrument.

4. Necessary Ground Truth

[20] In the face of the attractive and unique advantage of observing surface erosion of EB by IS via SHEA, we caution the need for minimizing the uncertainties from the complexity of the surface being bombarded by ions of different species and energy and ejecting SHEA of different species and energies. This prerequisite for extracting information reliably from the three sets of data—incident ion fluxes, surface composition, and SHEA maps—must be guided by solid ground truths found only in extensive laboratory data on sputtering mechanisms and yields.

[21] Quantitative laboratory simulations and computer modeling of IS occurring on EB are essential for understanding SHEA data from planetary missions. This is analogous to the need for ground truth in remote sensing: only on-site measurements that help calibrate aerial photographs and satellite imagery can make data interpretation and anal-

ysis credible. It has been suggested that measurements of composition and kinetics of atoms and molecules in a body's exosphere during an orbiting mission could determine the importance of the different surface release mechanisms, and the surface composition [e.g., *Johnson et al.*, 1998]. In particular, the IS process will require laboratory measurements to support existent and future planetary missions. We cite here some existing use of theoretical knowledge of IS on space data (see Appendix A), and where laboratory data are needed to resolve complexities that theory alone proves difficult.

[22] As mentioned in section 2, the ejection of surface atoms or molecules by IS is characterized by the yield Y. At projectile energies of the order keV, e.g., SW, IS occurs due to electronically elastic knock-on (ballistic) processes that are fairly well described by the linear cascade theory [*Sigmund*, 1969]. For certain insulators, the electronic excitations produced by the projectile can live long enough to produce what is known as electronic sputtering [*Johnson*, 1990]. The relative importance of these two processes depends on ion velocity and charge state.

[23] According to the standard linear collision cascade theory, the elastic sputtering yield for atomic targets is proportional to the ratio of the energy deposited at the surface and the binding energy of the surface atoms. This concept has been widely used to estimate the contribution of sputtering to the exosphere of Mercury, the Moon, the NEO and the Jupiter moons [*Wurz and Lammer*, 2003; *Massetti et al.*, 2003; *Leblanc et al.*, 2007; *Mura et al.*, 2009; *Plainaki et al.*, 2009, 2010]. Concerning this last case, the sputtering is much more complex, since electronic sputtering occurs. In fact, this process is very effective in materials with low cohesive energies such as the frozen gases in the outer solar system, often referred to as "ices." For such materials the total electronic sputtering yield Y is often proportional to the square of the electronic stopping cross section. Early laboratory sputtering data by *Brown et al.* [1982] were used to predict the principal atmospheric component of Europa, O_2, and its average column density [*Johnson et al.*, 1982]. In addition, the predicted large sputtering yields have led to the suggestion that other trace species should be present [*Johnson et al.*, 1998].

[24] Electronic sputtering is closely related to desorption induced by electronic transitions (DIET) [e.g., *Madey et al.*, 2002]. In DIET, an incident electron, ion or photon excites a surface state, which can relax by ejecting an ion or a neutral. This is a process that is linear in the excitation cross sections and is responsible for the sodium atmospheres on Mercury and the Moon [*Yakshinskiy and Madey*, 2000]. The DIET process occurring on Mercury and the Moon is molecularly specific and is, therefore, efficient for specific trace species (primarily the alakalis) or molecules adsorbed on refractory surfaces. Energetic electrons, ions or photons can produce deep excitations which, in principal, can result in the ejection of a large variety of surface species. However, such excitation events typically occur with lower probability. The interest in knock-on sputtering is that it is more robust and could eject into the gas phase species that are more representative of the surface composition. With the discovery of calcium ejected from Mercury's surface, this would appear to be born out. However, predictions for bodies with silicate surfaces, like the Moon [*Johnson and Baragiola*, 1991], have been much less successful than is the case for the icy bodies discussed above. This fact is primarily because the yields are small ($\ll$1 atom per ion), e.g., for SW bombardment, so that the sputtering of an element is more sensitive to its molecular surroundings, and, as discussed below, there is insufficient data on refractory planetary materials. In attempting to model this process, there are several reasons that would discourage the use of the linear cascade theory to estimate the elastic sputtering yield contribution to the planetary exospheres as currently being applied in atmospheric models. The theory was developed for monoatomic targets, it assumes a constant binding energy for atoms at the surface, and since it is based on a transport theory approximation, it only works for amorphous materials. Of critical importance in planetary science is the so-called "threshold regime," where the model breaks down and empirical models are used.

[25] Sputtering becomes even more complex, if the target consists of two or more different atomic species. The complication arises because the energy transfer from the projectile to the various target species is different. More important, each species has a different binding energy to the lattice and, therefore, irradiation leads to enhanced diffusion and depletion of the more volatile species resulting in a change of the composition of the solid with depth.

[26] Sputtering yields are usually measured on relatively flat laboratory surfaces. However, meteoritic bombardment over millions or billions of years on the surface of an astronomical body produces a regolith, a porous surface composed of grains formed by cumulative fracture and crater ejecta. Ions impact a regolith structure over a range of incident angles. Since the sputtering yield depends steeply on the local incidence angle θ (for ices the standard linear cascade theory predicts a dependence of $\cos^{-f}\theta$, where f is between 1 and 2 and is nearly independent of the projectile energy [*Famá et al.*, 2008]), one would expect that the yield from a regolith would be different compared to a hypothetical flat surface. This effect has been evaluated using Monte Carlo simulations by *Cassidy and Johnson* [2005], who found that the total sputtering could be significantly lower than the laboratory yields.

[27] In contrast with the numerous studies of the sputtering of water ice [see *Baragiola et al.*, 2003; *Famá et al.*, 2008, and references therein], which have been of useful application for analysis of outer planetary systems [e.g., *Johnson et al.*, 2008], there are few laboratory measurements of sputtering of neutrals and secondary ions from minerals [*Betz and Wehner*, 1983; *Jull et al.*, 1980; *Elphic et al.*, 1991; *Betz and Wien*, 1994; *Wiens et al.*, 1997]. Therefore, measuring sputtering rates and velocity distributions of sputtered species from minerals and ices relevant to planetary surfaces is essential to support SHEA data from future planetary missions. Because such measurements are time intensive and can often not be made over the full energy range required, simulations of sputtering are critical for extending the range of applicability, especially in the threshold region. Both Monte Carlo test particle simulations and Molecular Dynamics simulations have been carried out. The Monte Carlo simulations, typically only track recoils with energies much greater than the cohesive energy of the solid, and necessarily give results equivalent to those obtained from the linear Boltzmann equations. The best known of such calculations are the heavily used TRIM/SRIM models (see section 2). However, these are applicable only in regions in

which linear cascade model is valid and fail in the threshold regime. Much more useful are the Molecular Dynamics methods which are, of course, much more computationally intensive. In such models the atoms and/or molecules in the materials interact with each other and with the incoming ions via intermolecular potentials. To date, they have been primarily applied to model materials [*Tucker et al.*, 2005; *Bringa et al.*, 2000], but extensions to materials with compositions and properties similar to surfaces of the Moon and Mercury are feasible. Because the intermolecular potentials are not known in details for complex materials, both types of simulations are typically calibrated to experiment. Therefore, they are primarily useful as means for extending the range of the available data. This combination of laboratory experiments and numerical simulations will be essential to support the proposed SHEA instrumentation and mission design.

5. Conclusion

[28] In the interest of understanding what kind of evolution led to the present composition of planetary atmospheres, including that of Earth, we need to learn how the current rates of the ongoing processes that cause surface modifications and particle escapes vary under different conditions. To begin, we suggest concentrating on planets, moons and small bodies that are not protected by either strong magnetic fields or thick atmospheres, i.e., EB (exposed bodies). Furthermore, we identified IS (ion sputtering) on EB as the first process for detailed investigation for the following three reasons.

[29] 1. Incessant bombardment by either SW (solar wind) or MS (magnetospheric) ions on the respective EB constitutes predominant relevant process in altering the surface and consequently the associated ground-hugging exosphere.

[30] 2. The ejected products of IS on the surface, SHEA (sputtered high-energy atoms), are mostly neutral and energetic enough not only to be distinct from surface-released particles from other processes, but also to escape local gravity and magnetic field for remote sensing.

[31] 3. Remote sensing in SHEA can provide mapping of the EB under IS with temporal and mass resolution.

[32] We illustrated what is possible and what is needed to realize remote sensing IS on EB in SHEA. In Appendix A, referenced computer simulations using existing sputtering data and realistic EB models are shown. We hope this paper has initiated the drive toward determining how the rates of the ongoing IS processes that cause the changes vary under different SW and MS conditions.

[33] For such an effort, we see that parallel to planning flyby or orbiter missions to EB and developing SHEA instrumentation (e.g., BepiColombo/SERENA/ELENA [*Orsini et al.*, 2009b, 2010]) for such missions, performing sputtering experiments in the laboratories using appropriate incident ions and impacting surface analogs is equally necessary. The latter would indeed produce data crucial for the planning of the missions and design of SHEA instruments as well as for extracting factual information from the ensuing SHEA data.

Appendix A: Simulations

[34] Based on currently available IS data and theoretical models of EB, we present here material extracted from recently published papers, on what could be expected from SHEA imaging, by simulation of the following EB in their particular environments: Mercury, when the interplanetary magnetic field (IMF) configurations and SW conditions permit the plasma to reach the planetary surface (section A1); the Moon, in the SW while outside the Earth magnetosphere, or when it crosses the plasma sheet (section A2); asteroids and small bodies continuously exposed to the solar wind plasma (section A3); and the Jovian moons, Europa and Ganymede, when embedded in the Jupiter magnetosphere radiation belts (section A4).

A1. Mercury

[35] SHEA measurements of Mercury should be particularly intriguing, since they would give the opportunity to investigate the MS and planet interaction with the intense SW flux at about 0.3 AU. Many authors [e.g., *Killen et al.*, 2001; *Sarantos et al.*, 2001; *Kallio and Janhunen*, 2003; *Massetti et al.*, 2003] showed that under specific IMF configurations, SW can enter through the cusps in the dayside MS, eventually reaching the surface at midlatitudes. Under different IMF conditions, the configuration of the Hermean MS changes so that the area of high proton precipitation (hence: of subsequent SHEA release) moves accordingly [e.g., *Sarantos et al.*, 2001; *Kallio and Janhunen*, 2004; *Massetti et al.*, 2007]. Ground-based observations, indeed frequently indicate midlatitude exospheric Na densities to vary over time scales of hours [*Leblanc and Johnson*, 2010]. The nature of such variations is still unresolved, but it appears to be related to plasma precipitating regions [*Orsini et al.*, 2007; *Mura et al.*, 2005; *Leblanc et al.*, 2007; *Mura et al.*, 2009].

[36] The main constituents of the Hermean exosphere are probably volatiles released thermally or by PSD. Not contained in the exosphere, but directly ejected and escaping the gravity will be the flux of SHEA. The sensor ELENA [*Orsini et al.*, 2009b], part of the SERENA particle package [*Orsini et al.*, 2010] on board BepiColombo ESA-JAXA mission (launch 2014 [*Benkhoff et al.*, 2010]), will permit for the first time to map the IS emission, less intense than the PSD emission, but more effective in releasing refractories from the Hermean surface [*Milillo et al.*, 2005]. The flux of ~1–5 keV SW protons hitting the Hermean surface is estimated $\sim 10^9$ cm^{-2} s^{-1}; a total sputtering yield ~10% of the incident ion flux would lead to a total sputtered flux $\sim 10^8$ cm^{-2} s^{-1}. Approximately 50% of the ejected particles escape the planet along ballistic trajectories; and ~1% of these particles have enough energy (>20 eV) to be detected by the ELENA sensor. For comparison, the backscattering flux is of the same order of magnitude as that of the sputtered signal, but with an energy spectrum at higher energies. Figure A1 (top left) shows simulated total sputtered flux from Mercury's surface over the northern hemisphere [*Mura et al.*, 2005]. The portion of the surface seen in SHEA from a vantage point at 400 km altitude, latitude 45° and LT 1200, is illustrated in Figure A1 (bottom left).

[37] As BepiColombo Mercury Planetary Orbiter (MPO, where SERENA will be mounted) will fly over Mercury at low altitudes (orbit: 400 × 1550 km [see *Benkhoff et al.*, 2010]), ELENA's narrow field of view (4° × 76°, with 4° × 4° resolution) will ground track Mercury's surface in SHEA along the MPO orbital path, as shown in Figure A1 (top

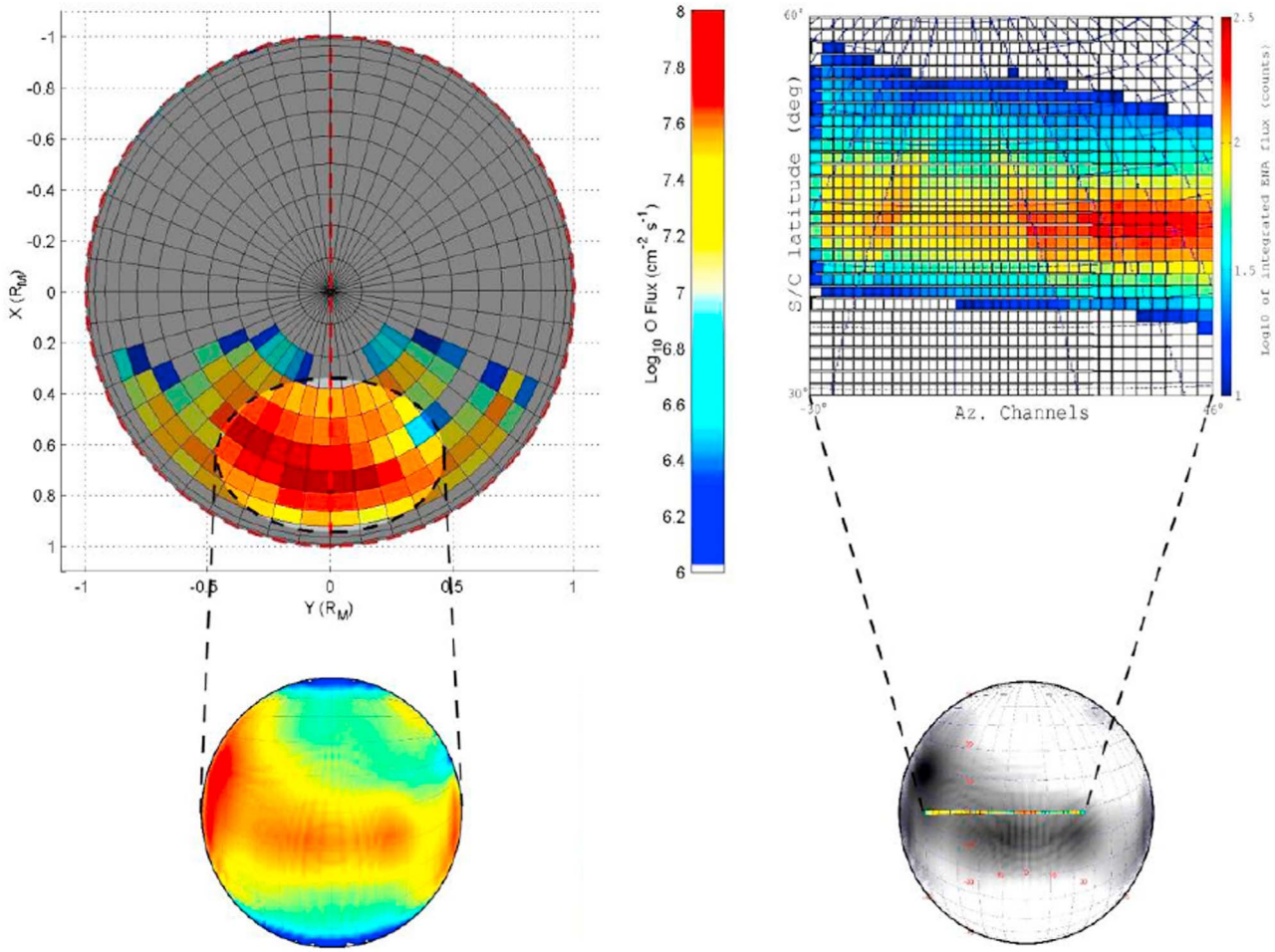

Figure A1. (top left) Pseudocolor map of SHEA flux from the northern surface of Mercury due to proton sputtering [from *Mura et al.*, 2005]. The oval-shaped dotted line is the horizon as seen from the s/c (400 km above surface level). (bottom left) SHEA signal as seen from the s/c. (bottom right) ELENA field of view and count rate (color) superimposed to the SHEA signal (gray). (top right) Thanks to the s/c motion, the ground track of ELENA data allows global imaging of the surface SHEA emission.

right). Figure A1 (bottom right) puts a single scan in perspective to the SHEA emitting region shown in Figure A1 (bottom left).

[38] Eventually, SHEA imaging by ELENA will map the proton precipitation regions, with the help of the simultaneous detection of the backscattered neutrals, with surface spatial resolution between 15 and 50 km, depending on s/c altitude. Simulations show that ELENA's spatial and time resolution capability will allow monitoring the dynamical behavior of the magnetospheric configuration; whereas its spatial resolution of tens km will allow to discriminate surface emissivity variations: as explained in section 4, the intensity of the directional SHEA signal depends on both ion precipitation flux and surface properties, like composition and intrinsic sputtering yield.

A2. The Moon

[39] The relative importance of IS as a source process for the lunar exosphere remains questionable, despite the extensive telescopic observations of Na on the Moon. This is due to the limitations of the viewing geometry from Earth. The Na emission clearly decreases when the Moon lies inside the terrestrial magnetosphere as would be consistent with a substantial reduction of ion precipitation contribution to this process [e.g., *Potter and Morgan*, 1994], but this decrease coincides with a changing line of sight: the observer at or close to full Moon is limited to observing the terminator limb, where flux-dependent sources are weak. As a result, interpretation of the existing ground-based data must necessarily rely on transport models, which account for this geometrical effect.

[40] Solar wind proton sputtering of Na (Figure A2) is suggested to be unimportant under the assumption of yields 0.01–0.1 per ion, contributing ~1% of the total sodium exosphere. Based on the yields for desorption induced by electronic transition processes that are measured in laboratory studies [e.g., *Madey et al.*, 1998, 2002], PSD is the dominant sodium source process, while vaporization of regolith material caused by MIV has been suggested to constitute up to 50% of the local density of sodium at the terminator, although models may disagree [e.g., *Leblanc and Johnson*, 2010]. For

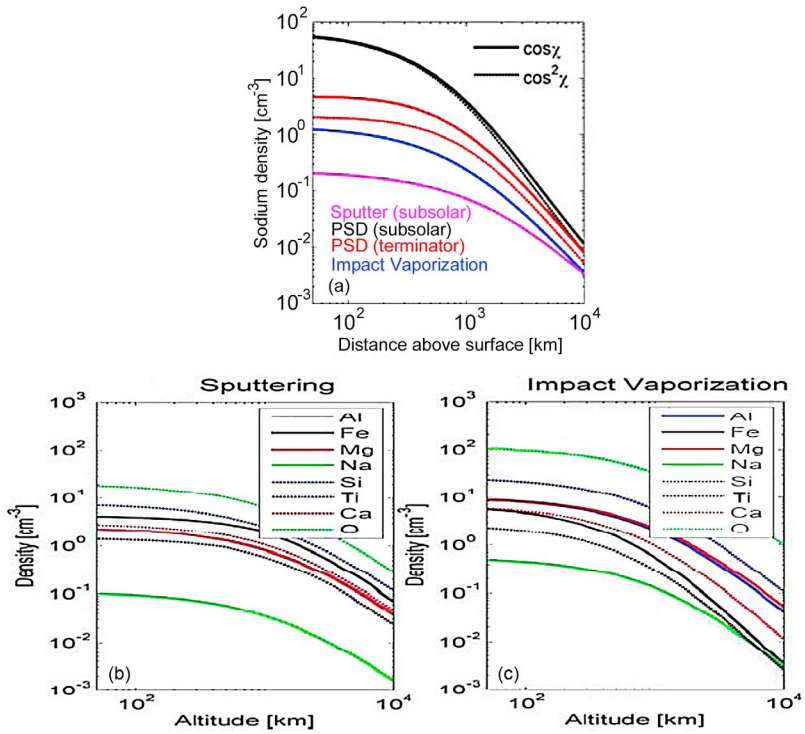

Figure A2. Model of the equatorial lunar exosphere: (a) sodium density and its variation with solar zenith angle, χ, and altitude for PSD, MIV, and IS; (b and c) subsolar point profiles attributed to IS and MIV for a number of other abundant lunar constituents.

refractory species, which remain undetected as neutrals, yet have been identified as pickup ions [*Mall et al.*, 1998; *Yokota et al.*, 2009], impact vaporization is expected to be the dominant source process, although ejection in the form of molecular oxides and their subsequent photodissociation remains a candidate [*Morgan and Killen*, 1997]. However, considerable uncertainties still exist regarding both the flux of micrometeoroids at 1 AU [*Cintala*, 1992; *Love and Brownlee*, 1993] and the effect of multiply charged solar wind heavy ions, which are common during Coronal Mass Ejection (CME) events. In situ SHEA measurements are needed to constrain the sputtering source. Furthermore, the detection of asymmetries in backscattered fluxes linked to magnetic anomalies (observed by *Wieser et al.* [2010]) allows remote sensing of the effects of SW interaction with the micromagnetospheres due to local magnetism. Simultaneous observation of IS emission in SHEA would add necessary details on surface-SW interaction.

[41] The sputtered density of the major species of the lunar regolith (O, Al, Si, Mg, …) is shown in Figure A2b. Sputter yields and elemental abundances consistent with *Wurz et al.* [2007] were assumed. At 50 km where a possible orbiter could be located, all the IS species (mainly O and Si) have densities of the order of 4 cm^{-3} in agreement with the estimation of *Milillo et al.* [2011]. This flux might increase following the exposure of the lunar surface to Earth's plasma sheet ions, which impart approximately three times higher energy than SW ions. Measured enhancements of the sodium exosphere at full Moon have been correlated to such plasma sheet crossings [*Wilson et al.*, 2006; *Sarantos et al.*, 2008].

A3. Asteroids and Small Bodies

[42] Asteroids suffer erosion and surface alteration from SW and solar and galactic cosmic ray bombardment, as well as from solar photon irradiation and micrometeorites gardening. Consequently, the relevant surface release processes, when they are within few AU from the Sun, are IS, PSD and MIV. TD is strongly temperature dependent; hence, its contribution to exosphere generation becomes important only at about 1 AU from the Sun, and increases when moving toward perihelion. The detection and analysis of SHEA from asteroids separates IS from the contribution from other release processes, thus SHEA detection would enable speculating on the surface erosion under different environmental conditions. SW sputtering investigation provides important clues on the evolution of a planetary body.

[43] Solar wind precipitation on the surface of an asteroid can be strongly influenced by the presence of magnetic fields. This seems to be the case of Vesta; in fact, *Vernazza et al.* [2006] identified a lower limit of $3 \cdot 10^{16}$ A m^2 for eventual possible Vesta magnetic dipole, capable to deviate the solar wind away from its surface. Not only a dipole can deviate SW from hitting the surface of an asteroid, but also smaller magnetic structures, known as minimagnetospheres [*Winglee et al.*, 2000], similarly to what has been imaged at the Moon in backscattered neutral atoms, showing a reduction of neutral flux from the surface corresponding to a strong magnetic anomaly [*Wieser et al.*, 2010]. The possible presence of such magnetic structures can cause a reduction of the SHEA flux released from an asteroid, thus minimizing local erosion and surface alteration effects.

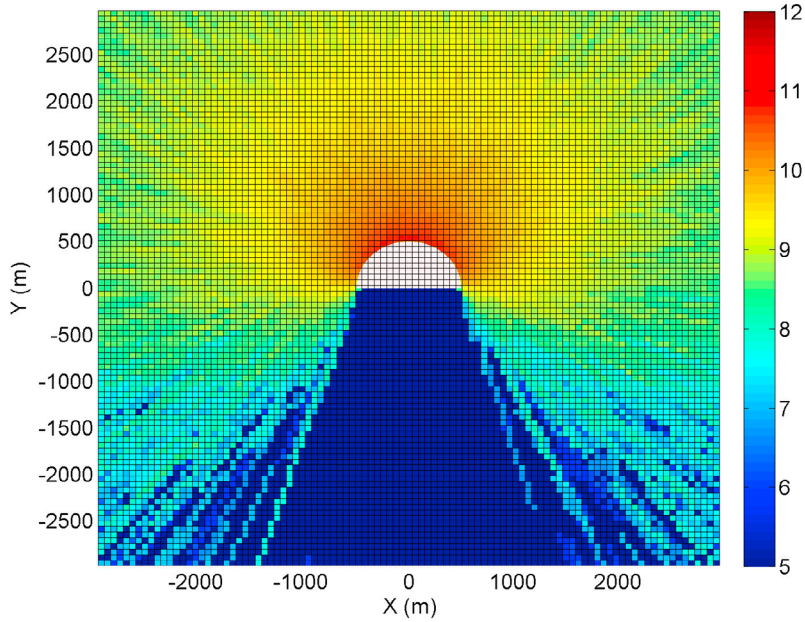

Figure A3. Simulated integral flux (log(particles m^{-2} s^{-1})) of total sputtered particles from CI chondrites NEO for impinging protons of energy ~1 keV. Axial symmetry is assumed; positive *Y* points to the Sun [*Plainaki et al.*, 2009].

[44] A study on asteroids' exosphere based on the simulation of the various release processes on the surface of the body has been performed by *Schläppi et al.* [2008], for the asteroids (2867) Steins and (21) Lutetia, in preparation of the Rosetta flybys. They found SW sputtering to be the most important exospheric supply process on the sunlit side of an asteroid. At the near Earth distances, IS is expected to be even more significant.

[45] The escape velocity of a Near Earth Object (NEO) is very low (i.e., 0.52 m/s for a NEO of mass ~10^{12} kg and of radius ~0.5 km), the particles released from the surface of a NEO are, therefore, essentially lost in space. Given a specific model for the simulation of the various release processes happening on the surface of a NEO, the efficiency of each of the particle release processes can be estimated. Clearly, identifying the NEO surface properties and its interactions

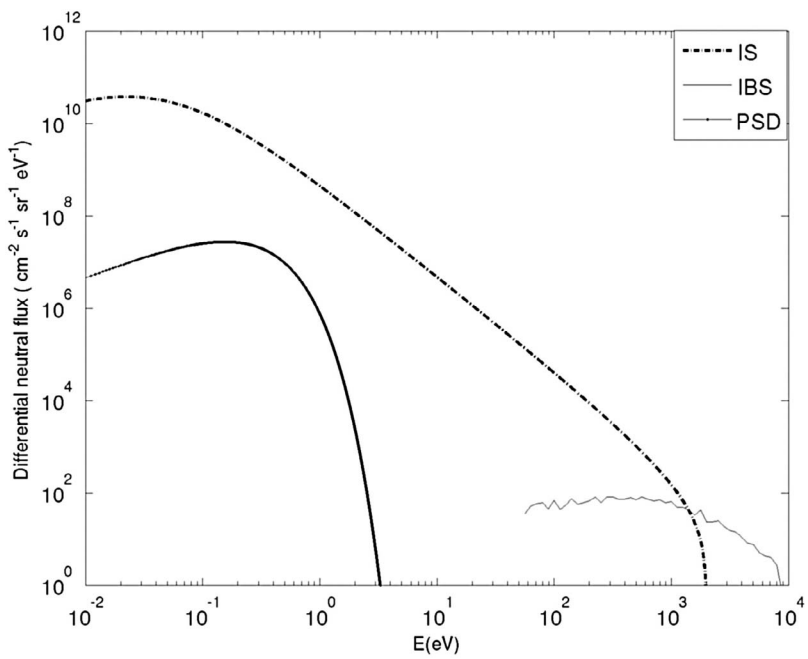

Figure A4. Intensity versus energy spectrum of the sputtered, backscattered, and PSDed neutrals at Europa [*Plainaki et al.*, 2010].

Table A1. Sputtered Escape Fraction From Reference EB

EB	Exposed Surface (%)	Escaping Sputtered Fraction (%)
Mercury	25	70
Moon (out of Earth's magnetosphere)	50	90
NEO	50	100
Europa	100	22

with SW can provide important information on the effects of space weathering on localized surface regions as well as the global evolution history of the body.

[46] *Plainaki et al.* [2009] applied the Monte Carlo SPAce Weathering on NEOs (SPAWN) model to obtain the sputtered distribution around a NEO as a result of its exposure to SW (Figure A3). They found that significant sputtered fluxes could reach a maximum value of 10^{11} particles m^{-2} s^{-1} around the NEO. The major component of sputtered species is expected to be H. The simulated density, produced by all species of sputtered particles emerging from a NEO surface, is calculated to be $\sim 3 \cdot 10^6$ particles m^{-3} near the NEO surface. The expected SHEA (E > 10 eV) fraction results in ~1% of the total released particles. On the other hand, the contribution to the total density of the volatiles emerging from the NEO surface, via the PSD process, is $\sim 1 \cdot 10^8$ particles/m^3.

[47] The global analysis of the sputtering erosion of the NEO surface would provide unique information about the present and the past of the NEO's surface, revealing the mechanism through which the solar wind has interacted with the surface atoms, in the past millions of years.

A4. Europa and Other Jovian Moons

[48] The radiation environment of Europa consists of intense H^+, O^+, S^+, and C^+ ion fluxes, in the energy range from keV to MeV (peaking at ~100 keV). These ions can erode the surface of Europa via ion sputtering, ejecting up to 1000 H_2O molecules per incident ion, and also break the chemical bonds of the ejected species resulting in the formation of new molecules (e.g., O_2), a process called radiolysis. The neutrals produced have a characteristic spectrum [*Cooper et al.*, 2001; *Strazzulla et al.*, 2003; *Paranicas et al.*, 2002]. *Plainaki et al.* [2010] found that the most significant sputtered H_2O emerging flux and density come from impinging S^+ ions, and they amount to 66% and 59% of the total ($3.2 \cdot 10^{13}$ H_2O m^{-2} s^{-1} and $2.7 \cdot 10^{10}$ H_2O/m^3, respectively). The total sputtering rate for Europa was calculated to be $\sim 10^{27}$ H_2O/s with escaping ratio 22%. This value, locally on the moon's surface, may exhibit variations; probably, it is higher in the trailing face, where the precipitation is foreseen to be more intense. In fact, this result is inside the range for the Europa loss rate given in literature and ranging between a few 10^{26} H_2O s^{-1} and 10^{28} H_2O s^{-1} [*Lanzerotti et al.*, 1982; *Johnson et al.*, 1981; *Eviatar et al.*, 1981, 1985; *Shi et al.*, 1995; *Ip*, 1996]. A similar result is also derived by the Energetic Particle Detector (EPD) data on the Galileo mission, $1.1 \cdot 10^{26}$ atoms/s [*Ip et al.*, 1998].

[49] Estimated energy spectra for IS, PSD, and ion backscattering (IBS) processes on Europa are shown in Figure A4 [*Plainaki et al.*, 2010]. Clearly, IS is far more productive, hence, SHEA dominates over releases from IBS (mainly H) and PSD at energies <1 keV.

[50] The slightly lower incident ion fluxes and the similarity between Ganymede and Europa in surface composition, drives the conclusion that slightly less SHEA fluxes are expected at Ganymede, where the internal magnetic field is not able to shield the plasma [*Kivelson et al.*, 2002]. Callisto, on the other hand, is considerably out of Jupiter's radiation belt; hence, the expected SHEA flux should be considerably lower in nominal conditions. A comparative detection of SHEA from these three Jovian moons would be of particular interest in the study of Jupiter system's evolution.

[51] At Mercury, 1 keV solar wind H ions release various types of atoms (like Na, Ca, K, Mg), and probably some molecules, too. Binding energies of these species with the surface of the planet are between 1 and few eVs. At the Galilean moons, 100 keV H, O and S ions of Jupiter's magnetospheric plasma, release mainly H_2O. The sputtered particle energy distributions for molecular ices tend to have maxima at lower energies of about 0.05 eV [*Boring et al.*, 1984; *Haring et al.*, 1984]. Simulations of ion sputtering show that at Europa and Mercury in the precipitation areas, the fluxes of the released particles differ at about 1 order of magnitude (10^9 particles/cm^2/s at Europa [*Plainaki et al.*, 2010] and 10^8 particles/cm^2/s at Mercury [*Mura et al.*, 2005]). However, according to *Cassidy and Johnson* [2005], in the non-ice regions of Europa, the regolith can significantly modify the relative populations of atmospheric species and their spatial distributions across the surface. Consequently, the sputtering yields should be reduced due to sticking of sputtered species to neighboring grains [*Hapke*, 1986; *Johnson*, 1989] and therefore lower fluxes of sputtered particles would be expected.

[52] Estimated escape fractions of sputtered particles from the different environments and the rough fraction of exposed bodies surfaces considered in this review are summarized in Table A1.

[53] **Acknowledgments.** This paper is supported by the Italian Space Agency I-081-09-0 agreement for the BepiColombo/SERENA scientific activity. The comprehensiveness and quality of this paper are made possible by the critical reading and advice of G. Ho, M. Hilchenbach, and S. Selci.

[54] Masaki Fujimoto thanks the reviewers for their assistance in evaluating this paper.

References

Baragiola, R. A., R. A. Vidal, W. Svendsen, J. Schou, M. Shi, D. A. Bahr, and C. L. Atteberry (2003), Sputtering of water ice, *Nucl. Instrum. Methods Phys. Res.*, *209*, 294–303, doi:10.1016/S0168-583X(02)02052-9.

Benkhoff, J., J. van Casteren, H. Hayakawa, M. Fujimoto, H. Laakso, M. Novara, P. Ferri, H. R. Middleton, and R. Ziethe (2010), BepiColombo—Comprehensive exploration of Mercury: Mission overview and science goals, *Planet. Space Sci.*, *58*, 2–20, doi:10.1016/j.pss.2009.09.020.

Betz, G., and G. K. Wehner (1983), Sputtering of multi-component materials, in *Sputtering by Particle Bombardment II*, edited by R. Behrisch, pp. 11–90, Springer, Berlin.

Betz, G., and K. Wien (1994), Energy and angular distributions of sputtered particles, *Int. J. Mass Spectrom. Ion Processes*, *140*, 1–110, doi:10.1016/0168-1176(94)04052-4.

Bhardwaj, A., S. Barabash, Y. Futaana, Y. Kazama, K. Asamura, R. Sridharan, M. Holmström, P. Wurz, and R. Lundin (2005), Low energy neutral atom imaging on the Moon with the SARA instrument aboard Chandrayaan-1 mission, *J. Earth Syst. Sci.*, *114*(6), 749–760, doi:10.1007/BF02715960.

Boring, J. W., J. W. Garrett, T. A. Cummings, R. E. Johnson, and W. L. Brown (1984), Sputtering of solid SO_2, *Nucl. Instrum. Methods Phys. Res.*, *1*, 321–326, doi:10.1016/0168-583X(84)90087-9.

Bringa, E. M., M. Jakas, and R. E. Johnson (2000), Spike models for sputtering: Effect of the surface and the material stiffness, *Nucl. Instrum. Methods Phys. Res.*, *762*, 164–165, doi:10.1016/S0168-583X(99)01068-X.

Brown, W. L., W. M. Augustyniak, E. Simmons, K. J. Marcantonio, L. J. Lanzerotti, R. E. Johnson, J. W. Boring, C. T. Reimann, G. Foti, and V. Pirronello (1982), Erosion and molecule formation in condensed gas films by electronic energy loss of fast ions, *Nucl. Instrum. Methods Phys. Res.*, *198*, 1–8, doi:10.1016/0167-5087(82)90043-6.

Bzowski, M., H. J. Fahr, and D. Rucinski (1996), Interplanetary neutral particle fluxes influencing the Earth's atmosphere and the terrestrial environment, *Icarus*, *124*, 209–219, doi:10.1006/icar.1996.0199.

Bzowski, M., E. Möbius, S. Tarnopolski, V. Izmodenov, and G. Gloeckler (2008), Density of neutral interstellar hydrogen at the termination shock from Ulysses pickup ion observations, *Astron. Astrophys.*, *491*(1), 7–19, doi:10.1051/0004-6361:20078810.

Cassidy, T. A., and R. E. Johnson (2005), Monte Carlo model of sputtering and other ejection processes within a regolith, *Icarus*, *176*, 499–507, doi:10.1016/j.icarus.2005.02.013.

Cassidy, T. A., R. E. Johnson, and O. J. Tucker (2009), Trace constituents of Europa's atmosphere, *Icarus*, *201*, 182–190, doi:10.1016/j.icarus.2008.12.033.

Cintala, M. J. (1992), Impact-induced thermal effects in the lunar and Mercurian regoliths, *J. Geophys. Res.*, *97*, 947–973, doi:10.1029/91JE02207.

Cooper, J. F., R. E. Johnson, B. H. Mauk, H. B. Garrett, and G. Neil (2001), Energetic ion and electron irradiation of the icy Galilean satellites, *Icarus*, *149*, 133–159, doi:10.1006/icar.2000.6498.

Eichhorn, G. (1978), Heating and vaporization during hypervelocity particle impact, *Planet. Space Sci.*, *26*, 463–467, doi:10.1016/0032-0633(78)90067-3.

Elphic, R. C., H. O. Funsten III, B. L. Barraclough, D. J. McComas, M. T. Paffett, D. T. Vaniman, and G. Heiken (1991), Lunar surface composition and solar wind-induced secondary ion mass spectrometry, *Geophys. Res. Lett.*, *18*, 2165–2168, doi:10.1029/91GL02669.

Eviatar, A., G. L. Siscoe, T. V. Johnson, and D. L. Matson (1981), Effects of Io ejecta on Europa, *Icarus*, *47*, 75–83, doi:10.1016/0019-1035(81)90092-0.

Eviatar, A., A. Bar-Nun, and M. Podolak (1985), European surface phenomena, *Icarus*, *61*, 185–191, doi:10.1016/0019-1035(85)90100-9.

Falcone, G. (1990), Sputtering theory, *Riv. Nuovo Cimento Soc. Ital. Fis.*, *13*(1), 1–52.

Famá, M., J. Shi, and R. A. Baragiola (2008), Sputtering of water ice by low energy ions, *Surf. Sci.*, *602*, 156–161, doi:10.1016/j.susc.2007.10.002.

Gnaser, H. (2007), Energy and angular distributions of sputtered species, in *Sputtering by Particle Bombardments*, edited by R. Behrisch and W. Eckstein, pp. 231–328, Springer, Berlin, doi:10.1007/978-3-540-44502-9_5.

Goehlich, A., N. Niemöller, and H. F. Döbele (2000), Anisotropy effects in physical sputtering investigated by laser-induced fluorescence spectroscopy, *Phys. Rev. B*, *62*, 9349–9358, doi:10.1103/PhysRevB.62.9349.

Goettel, K. A. (1988), Present bounds on the bulk composition of Mercury: Implications for planetary formation processes, in *Mercury*, edited by F. Vilas, C. R. Chapman, and M. S. Matthews, pp. 613–621, Univ. of Ariz. Press, Tucson.

Hapke, B. (1986), On the sputter alteration of regoliths of outer solar system bodies, *Icarus*, *66*, 270–279, doi:10.1016/0019-1035(86)90157-0.

Hapke, B. (2001), Space weathering from Mercury to the asteroid belt, *J. Geophys. Res.*, *106*, 10,039–10,073, doi:10.1029/2000JE001338.

Haring, R. A., R. Pedrys, D. J. Oostra, A. Haring, and A. E. de Vries (1984), Reactive sputtering of simple condensed gases by keV ions. III. Kinetic energy distributions, *Nucl. Instrum. Methods Phys. Res.*, *5*, 483–488, doi:10.1016/0168-583X(84)90005-3.

Hofer, W. O. (1991), Angular, energy, and mass distribution of sputtered particles, in *Sputtering by Particle Bombardment*, edited by R. Behrisch and K. Wittmaack, pp. 15–90, Springer, Berlin.

Hsieh, K. C., and C. C. Curtis (1988), A model for the spatial and energy distributions of energetic neutral atoms produced within the Saturn/Titan plasma system, *Geophys. Res. Lett.*, *15*, 772–775, doi:10.1029/GL015i008p00772.

Ip, W. H. (1996), Europa's oxygen exosphere and its magnetospheric interaction, *Icarus*, *120*, 317–325, doi:10.1006/icar.1996.0052.

Ip, W.-H., D. J. Williams, R. W. McEntire, and B. H. Mauk (1998), Ion sputtering and surface erosion at Europa, *Geophys. Res. Lett.*, *25*, 829–832, doi:10.1029/98GL00472.

Johnson, R. E. (1989), Application of laboratory data to the sputtering of a planetary regolith, *Icarus*, *78*, 206–210, doi:10.1016/0019-1035(89)90077-8.

Johnson, R. E. (1990), *Energetic Charged-Particle Interactions With Atmospheres and Surfaces*, Springer, Berlin.

Johnson, R. E. (2002), Surface boundary layer atmospheres, in *Atmospheres in the Solar System: Comparative Aeronomy*, *Geophys. Monogr. Ser.*, vol. 130, pp. 203–219, AGU, Washington, D. C.

Johnson, R. E., and R. Baragiola (1991), Lunar surface: Sputtering and secondary ion mass spectrometry, *Geophys. Res. Lett.*, *18*, 2169–2172, doi:10.1029/91GL02095.

Johnson, R. E., L. J. Lanzerotti, W. L. Brown, and T. P. Armstrong (1981), Erosion of Galilean satellite surfaces by Jovian magnetosphere particles, *Science*, *212*, 1027–1030, doi:10.1126/science.212.4498.1027.

Johnson, R. E., L. J. Lanzerotti, and W. L. Brown (1982), Planetary applications of ion-induced erosion of condensed-gas frost, *Nucl. Instrum. Methods Phys. Res.*, *198*, 147–157, doi:10.1016/0167-5087(82)90066-7.

Johnson, R. E., R. M. Killen, J. H. Waite, and W. S. Lewis (1998), Europa's surface composition and sputter-produced ionosphere, *Geophys. Res. Lett.*, *25*, 3257–3260, doi:10.1029/98GL02565.

Johnson, R. E., M. Famá, M. Liu, R. A. Baragiola, E. C. Sittler Jr., and H. T. Smith (2008), Sputtering of ice grains and icy satellites in Saturn's inner magnetosphere, *Planet. Space Sci.*, *56*, 1238–1243, doi:10.1016/j.pss.2008.04.003.

Johnson, R. E., R. W. Carlson, T. A. Cassidy, and M. Famá (2011), Sputtering of ices, in *The Science of Solar System Ices*, *ScSSI Rev. Ser.*, edited by M. Gutipati and J. Castillo-Rogez, Springer, Berlin, in press.

Jull, A. J. T., G. C. Wilson, J. V. P. Long, S. J. B. Reed, and C. T. Pillinger (1980), Sputtering rates of minerals and implications for abundances of solar elements in lunar samples, *Nucl. Instrum. Methods*, *168*, 357–365, doi:10.1016/0029-554X(80)91276-8.

Kallio, E., and P. Janhunen (2003), Modelling the solar wind interaction with Mercury by a quasineutral hybrid model, *Ann. Geophys.*, *21*(11), 2133–2145, doi:10.5194/angeo-21-2133-2003.

Kallio, E., and P. Janhunen (2004), The response of the Hermean magnetosphere to the interplanetary magnetic field, *Adv. Space Res.*, *33*(12), 2176–2181, doi:10.1016/S0273-1177(03)00447-2.

Killen, R. M., and W.-H. Ip (1999), The surface-bounded atmospheres of Mercury and the Moon, *Rev. Geophys.*, *37*(3), 361–406, doi:10.1029/1999RG900001.

Killen, R. M., A. E. Potter, P. Reiff, M. Sarantos, B. V. Jackson, P. Hick, and B. Giles (2001), Evidence for space weather at Mercury, *J. Geophys. Res.*, *106*, 20,509–20,525, doi:10.1029/2000JE001401.

Killen, R., et al. (2007), Processes that promote and deplete the exosphere of Mercury, *Space Sci. Rev.*, *132*, 433–509, doi:10.1007/s11214-007-9232-0.

Kivelson, M. G., et al. (2002), The permanent and inductive magnetic moments of Ganymede, *Icarus*, *157*, 507–522, doi:10.1006/icar.2002.6834.

Krimigis, S. M., et al. (2004), Magnetosphere imaging instrument (MIMI) on the Cassini mission to Saturn/Titan, *Space Sci. Rev.*, *114*, 233–329, doi:10.1007/s11214-004-1410-8.

Lammer, H., P. Wurz, M. R. Patel, R. Killen, C. Kolb, S. Massetti, S. Orsini, and A. Milillo (2003), The variability of Mercury's exosphere by particle and radiation induced surface release process, *Icarus*, *166*, 238–247, doi:10.1016/j.icarus.2003.08.012.

Lanzerotti, L. J., W. L. Brown, W. M. Augustyniak, R. E. Johnson, and T. P. Armstrong (1982), Laboratory studies for charged particle erosion of SO_2 ice and applications to the frosts of Io, *Astrophys. J.*, *259*, 920–929, doi:10.1086/160225.

Leblanc, F., and R. E. Johnson (2010), Mercury exosphere I. Global circulation model of its sodium component, *Icarus*, *209*, 280–300.

Leblanc, F., et al. (2007), Mercury's exosphere origins and relations to its magnetosphere and surface, *Planet. Space Sci.*, *55*, 1069–1092, doi:10.1016/j.pss.2006.11.008.

Lindsay, B. G., and R. F. Stebbings (2005), Charge transfer cross sections for energetic neutral atom data analysis, *J. Geophys. Res.*, *110*, A12213, doi:10.1029/2005JA011298.

Love, S. G., and D. E. Brownlee (1993), A direct measurement of the terrestrial mass accretion rate of cosmic dust, *Science*, *262*, 550–553, doi:10.1126/science.262.5133.550.

Madey, T. E., B. V. Yakshinskiy, V. N. Ageev, and R. E. Johnson (1998), Desorption of alkali atoms and ions from oxide surfaces—Relevance to origins of NA and K in atmospheres of Mercury and the Moon, *J. Geophys. Res.*, *103*, 5873–5887, doi:10.1029/98JE00230.

Madey, T. E., R. E. Johnson, and T. M. Orlando (2002), Far-out surface science: Radiation-induced surface processes in the solar system, *Surf. Sci.*, *500*, 838–858, doi:10.1016/S0039-6028(01)01556-4.

Mall, U., E. Kirsch, K. Cierpka, B. Wilken, A. Söding, F. Neubauer, G. Gloeckler, and A. Galvin (1998), Direct observation of lunar pick-up ions near the Moon, *Geophys. Res. Lett.*, *25*, 3799–3802, doi:10.1029/1998GL900003.

Massetti, S., S. Orsini, A. Milillo, A. Mura, E. De Angelis, H. Lammer, and P. Wurz (2003), Mapping of the cusp plasma precipitation on the surface of Mercury, *Icarus*, *166*, 229–237, doi:10.1016/j.icarus.2003.08.005.

Massetti, S., S. Orsini, A. Milillo, and A. Mura (2007), Modelling Mercury's magnetosphere and plasma entry through the dayside magnetopause, *Planet. Space Sci.*, *55*, 1557–1568, doi:10.1016/j.pss.2006.12.008.

McComas, D. J., et al. (2009), Lunar backscatter and neutralization of the solar wind: First observations of neutral atoms from the Moon, *Geophys. Res. Lett.*, *36*, L12104, doi:10.1029/2009GL038794.

Milillo, A., et al. (2005), Surface-exosphere-magnetosphere system of Mercury, *Space Sci. Rev.*, *117*, 397–443, doi:10.1007/s11214-005-3593-z.

Milillo, A., et al. (2011), Exosphere generation of the Moon investigated through a high energy neutral detector, *Exp. Astron.*, doi:10.1007/s10686-010-9196-z, in press.

Morgan, T. H., and R. M. Killen (1997), A non-stoichiometric model of the composition of the atmospheres of Mercury and the Moon, *Planet. Space Sci.*, *45*, 81–83, doi:10.1016/S0032-0633(96)00099-2.

Mura, A., S. Orsini, A. Milillo, D. Delcourt, and S. Massetti (2005), Dayside H^+ circulation at Mercury and neutral particle emission, *Icarus*, *175*, 305–319, doi:10.1016/j.icarus.2004.12.010.

Mura, A., P. Wurz, H. I. M. Lichtenegger, H. Schleicher, H. Lammer, D. Delcourt, A. Milillo, S. Massetti, M. L. Khodachenko, and S. Orsini (2009), The sodium exosphere of Mercury: Comparison between observations during Mercury's transit and model results, *Icarus*, *200*, 1–11, doi:10.1016/j.icarus.2008.11.014.

Orsini, S., L. G. Blomberg, D. Delcourt, R. Grard, S. Massetti, K. Seki, and J. Slavin (2007), Magnetosphere-exosphere-surface coupling at Mercury, *Space Sci. Rev.*, *132*, 551–573, doi:10.1007/s11214-007-9221-3.

Orsini, S., A. Mura, A. Milillo, V. Mangano, C. Plainaki, E. de Angelis, S. Massetti, G. Rinaldi, and R. Rispoli (2009a), The influence of space environment on the evolution of Mercury, *Eos Trans. AGU*, *90*(52), Fall Meet. Suppl., Abstract P21A-1203.

Orsini, S., et al. (2009b), Low energy high angular resolution neutral atom detection by means of micro-shuttering techniques: The BepiColombo SERENA/ELENA sensor, *AIP Conf. Proc.*, *91*, 1144–1155.

Orsini, S., et al. (2010), SERENA: A suite of four instruments (ELENA, STROFIO, PICAM and MIPA) on board BepiColombo-MPO for particle detection in the Hermean environment, *Planet. Space Sci.*, *58*, 166–181, doi:10.1016/j.pss.2008.09.012.

Paranicas, C., J. M. Ratliff, B. H. Mauk, C. Cohen, and R. Johnson (2002), The ion environment near Europa and its role in surface energetics, *Geophys. Res. Lett.*, *29*(5), 1074, doi:10.1029/2001GL014127.

Plainaki, C., et al. (2009), Space weathering on near Earth objects based on neutral particle detection, *Planet. Space Sci.*, *57*, 384–392, doi:10.1016/j.pss.2008.12.002.

Plainaki, C., A. Milillo, A. Mura, S. Orsini, and T. Cassidy (2010), Neutral particle release from Europa's surface, *Icarus*, *210*, 385–395, doi:10.1016/j.icarus.2010.06.041.

Potter, A. E., and T. H. Morgan (1994), Variation of lunar sodium emission intensity with phase angle, *Geophys. Res. Lett.*, *21*, 2263–2266, doi:10.1029/94GL01702.

Reimann, C. T., J. W. Boring, R. E. Johnson, J. W. Garrett, K. R. Farmer, and W. L. Brown (1984), Ion-induced molecular ejection from D2O ice, *Surf. Sci.*, *147*, 227–240.

Saito, Y., et al. (2008), Solar wind proton reflection at the lunar surface: Low energy ion measurement by MAP-PACE onboard SELENE (KAGUYA), *Geophys. Res. Lett.*, *35*, L24205, doi:10.1029/2008GL036077.

Sarantos, M., P. H. Reiff, T. H. Hill, R. M. Killen, and A. L. Urquhart (2001), A Bx-interconnected magnetosphere model for Mercury, *Planet. Space Sci.*, *49*, 1629–1635, doi:10.1016/S0032-0633(01)00100-3.

Sarantos, M., R. M. Killen, and J. A. Slavin (2008), The effect of solar wind impact on the lunar sodium emission, *Eos Trans. AGU*, *89*(23), Jt. Assem. Suppl., Abstract P34A-03.

Schläppi, B., K. Altwegg, and P. Wurz (2008), Asteroid exosphere: A simulation for the ROSETTA flyby targets (2867) Steins and (21) Lutetia, *Icarus*, *195*, 674–685, doi:10.1016/j.icarus.2007.12.021.

Shi, M., R. A. Baragiola, D. E. Grosjean, R. E. Johnson, S. Jurac, and J. Schou (1995), Sputtering of water ice surfaces and the production of extended neutral atmospheres, *J. Geophys. Res.*, *100*, 26,387–26,395, doi:10.1029/95JE03099.

Sieveka, E. M., and R. E. Johnson (1984), Ejection of atoms and molecules from Io by plasma-ion impact, *Astrophys. J.*, *287*, 418–426, doi:10.1086/162701.

Sigmund, P. (1969), Theory of sputtering. I. Sputtering yield of amorphous and polycrystalline targets, *Phys. Rev.*, *184*, 383–416, doi:10.1103/PhysRev.184.383.

Sigmund, P. (1981), Theoretical aspects of atomic mixing by ion beams, *Nucl. Instrum. Methods Phys. Res.*, *182–183*, 25–41, doi:10.1016/0029-554X(81)90668-6.

Strazzulla, G., G. Leto, O. Gomis, and M. A. Satorre (2003), Implantation of carbon and nitrogen ions in water ice, *Icarus*, *164*, 163–169, doi:10.1016/S0019-1035(03)00100-3.

Thompson, D. A. (1981), Application of an extended linear cascade model to the sputtering of Ag, Au, and Pt by heavy atomic and molecular ions, *J. Appl. Phys.*, *52*(2), 982–989.

Tucker, O. J., D. S. Ivanov, R. E. Johnson, L. V. Zhigilei, and E. M. Bringa (2005), Molecular dynamics simulation of sputtering from a cylindrical track: EAM versus pair potentials, *Nucl. Instrum. Methods Phys. Res.*, *228*, 163–169, doi:10.1016/j.nimb.2004.10.040.

Vernazza, P., R. Brunetto, G. Strazzulla, M. Fulchignoni, P. Rochette, N. Meyer-Vernet, and I. Zouganelis (2006), Asteroid colors: A novel tool for magnetic field detection? The case of Vesta, *Astron. Astrophys.*, *451*(3), L43–L46, doi:10.1051/0004-6361:20065176.

Wiens, R. C., et al. (1997), Sputtering products of sodium sulfate: Implications for Io's surface and for sodium-bearing molecules in the Io torus, *Icarus*, *128*, 386–397, doi:10.1006/icar.1997.5758.

Wieser, M., S. Barabash, Y. Futaana, M. Holmström, A. Bhardwaj, R. Sridharan, M. B. Dhanya, P. Wurz, A. Schaufelberger, and K. Asamura (2009), Extremely high reflection of solar wind protons as neutral hydrogen atoms from regolith in space, *Planet. Space Sci.*, *57*, 2132–2134, doi:10.1016/j.pss.2009.09.012.

Wieser, M., et al. (2010), First observation of a mini magnetosphere above a lunar magnetic anomaly using energetic neutral atoms, *Geophys. Res. Lett.*, *37*, L05103, doi:10.1029/2009GL041721.

Wilson, J. K., M. Mendillo, and H. E. Spence (2006), Magnetospheric influence on the Moon's exosphere, *J. Geophys. Res.*, *111*, A07207, doi:10.1029/2005JA011364.

Winglee, R. M., J. Slough, T. Ziemba, and A. Goodson (2000), Mini-magnetospheric plasma propulsion: Tapping the energy of the solar wind for spacecraft propulsion, *J. Geophys. Res.*, *105*, 21,067–21,078, doi:10.1029/1999JA000334.

Wurz, P., and H. Lammer (2003), Monte-Carlo simulation of Mercury's exosphere, *Icarus*, *164*, 1–13, doi:10.1016/S0019-1035(03)00123-4.

Wurz, P., et al. (2007), The lunar exosphere: The sputtering contribution, *Icarus*, *191*, 486–496, doi:10.1016/j.icarus.2007.04.034.

Yakshinskiy, B. V., and T. E. Madey (2000), Desorption induced by electronic transitions of Na from SiO_2: Relevance to tenuous planetary atmospheres, *Surf. Sci.*, *451*, 160–165, doi:10.1016/S0039-6028(00)00022-4.

Yokota, S., et al. (2009), First direct detection of ions originating from the Moon by MAP-PACE IMA onboard SELENE (KAGUYA), *Geophys. Res. Lett.*, *36*, L11201, doi:10.1029/2009GL038185.

Ziegler, J. F., J. P. Biersack, and U. Littmark (1966), *The Stopping and Range of Ions in Solids*, Pergamon, New York.

Zurbuchen, T. H., J. M. Raines, G. Gloeckler, S. M. Krimigis, J. A. Slavin, P. L. Koehn, R. M. Killen, A. L. Sprague, R. L. McNutt Jr., and S. C. Solomon (2008), MESSENGER observations of the composition of Mercury's ionized exosphere and plasma environment, *Science*, *321*(5885), 90–92, doi:10.1126/science.1159314.

R. Baragiola, M. Fama, and R. Johnson, Materials Science and Engineering, University of Virginia, Charlottesville, VA 22904, USA.

T. A. Cassidy, Jet Propulsion Laboratory, M/S 183-601, Pasadena, CA 91109, USA.

E. De Angelis, A. Milillo, A. Mura, S. Orsini, and C. Plainaki, INAF/IFSI, via del Fosso del Cavaliere, I-00133 Rome, Italy. (anna.milillo@ifsi-roma.inaf.it)

M. Desai, R. Goldstein, and S. Livi, Southwest Research Institute, PO Drawer 28510, San Antonio, TX 78228, USA.

K. C. Hsieh, Department of Physics, University of Arizona, Tucson, AZ 85721, USA.

W.-H. Ip, Department of Astronomy, National Central University, Jhongli 32001, Taiwan.

R. Killen, Planetary Magnetospheres Division, NASA GSFC, Code 695.0, Greenbelt, MD 20771, USA.

M. Sarantos, Heliophysics Division, NASA GSFC, Code 670.0, Greenbelt, MD 20771, USA.